Corrosion Science 149 (2019) 54–67

Contents lists available at ScienceDirect

Corrosion Science

journal homepage: www.elsevier.com/locate/corsci

The role of Sn on the long-term atmospheric corrosion of binary Cu-Sn bronze alloys in architecture

T. Chang[a,b], G. Herting[a], S. Goidanich[c], J.M. Sánchez Amaya[d], M.A. Arenas[e], N. Le Bozec[f], Y. Jin[b], C. Leygraf[a], I. Odnevall Wallinder[a,*]

[a] KTH Royal Institute of Technology, Division of Surface and Corrosion Science, School of Engineering Sciences in Chemistry, Biotechnology and Health, Dr. Kristinas v. 51, SE, 10044 Stockholm, Sweden
[b] National Center for Materials Service Safety, University of Science and Technology Beijing, Beijing 100083, China
[c] Politecnico di Milano, Department of Chemistry, Materials and Chemical Engineering "Giulio Natta", Via Mancinelli 7, 0131 Milan, Italy
[d] LABCYP, Department of Materials Science and Metallurgical Engineering and Inorganic Chemistry, School of Engineering, Avenida Universidad de Cadiz, 10, 11519 Puerto Real, Cádiz, Spain
[e] Departamento de Ingeniería de Superficies, Corrosión y Durabilidad, Centro Nacional de Investigaciones Metalúrgicas (CENIM/CSIC), Avenida de Gregorio del amo 8, 28040 Madrid, Spain
[f] French Corrosion Institute, 220 rue Pierre Rivoalon, 29200 Brest, France

ARTICLE INFO

Keywords:
Bronze
Atmospheric corrosion
Patina
Metal release
Aesthetic appearance

ABSTRACT

The role of Sn on the atmospheric corrosion performance of binary Cu-Sn bronze alloys (4–6 wt.% Sn) compared with Cu metal used in outdoor architecture is elucidated in terms of microstructure, native surface oxide composition, patina evolution, corrosion rates, appearance and metal release. Results are presented for non-exposed surfaces and surfaces exposed at different urban and marine sites in Europe up to 5 years and based on multi-analytical findings from microscopic, spectroscopic, electrochemical and chemical investigations. Alloying influenced the corrosion, aesthetic appearance and patina evolution, differently for urban and marine sites, whereas no effects were observed on the release pattern.

1. Introduction

Copper and copper-based alloys are common materials in ancient and modern architecture due to their aesthetic appearance, durability, corrosion resistance and possibility to recycle. The use of tin-bronze (Sn-bronze), brass and copper-aluminum alloys for roofing and facades is increasing in contemporary architecture. The use of bronze has a long tradition as the first alloy was developed already over 4000 years ago. Today, this group of materials includes a variety of alloys of different characteristics such as aluminum-bronze, phosphor-bronze, tin-bronze, silicon-bronze and manganese-bronze. Architectural bronze is a common alloy often referred to outdoor applications [1]. However, this is not a bronze alloy but rather a brass alloy that due to its aluminum content reveals a lustrous appearance. Sn-bronzes are due to their beneficial mechanical and physical properties (*e.g.* high yield strength, hardness, fatigue- and corrosion resistance) typically used in different applications such as in springs and bearings but low-Sn bronzes find an increasing use in modern architecture due to their surface appearance and corrosion resistance. Patination (weathering) and corrosion of different bronze alloys in architectural applications have, with the primary aim to preserve the cultural heritage [2–6], been studied over the last century in soil [3,4,7,8], in water or seawater [9–11], at atmospheric conditions [12,13] and in other aqueous corrosive media [14–17]. Atmospheric corrosion investigations of Sn-bronzes used for contemporary architecture are though scarce [18–22].

Cu-rich corrosion products have been reported to be the main patina constituents of bronze at atmospheric conditions [4,7,13,23]. At chloride-rich conditions, the patina evolution is consistent with findings for Cu metal [5,19,24], with the initial and continuous formation of cuprite (Cu_2O), followed by the formation of nantokite (CuCl) and subsequently its transformation to atacamite and/or its isomorphous phase paratacamite ($Cu_2(OH)_3Cl$). Patina formation on Cu metal in less sulfur-polluted environment, evolves via the formation of cuprite, followed by posnjakite ($Cu_4SO_4(OH)_6{\cdot}H_2O$) as a precursor to brochantite ($Cu_4SO_4(OH)_6$) [25]. At conditions with higher SO_2 levels, cuprite is followed by the formation of strandbergite ($Cu_{2.5}SO_4(OH)_3{\cdot}H_2O$), a precursor to antlerite ($Cu_3SO_4(OH)_4$) [25]. Sn-oxides (SnO_2, SnO and $SnO{\cdot}nH_2O$) have been identified within the patina on ancient bronzes

* Corresponding author.
E-mail address: ingero@kth.se (I. Odnevall Wallinder).

https://doi.org/10.1016/j.corsci.2019.01.002
Received 26 October 2018; Received in revised form 29 December 2018; Accepted 3 January 2019
Available online 06 January 2019

(Cu-Sn alloys) [3,26–29] of both relatively high (≥ 6 wt.%) [3,8] and low (˜1 wt.%) [30] Sn content.

Patina formation mechanisms of bronze artefacts have been elucidated by Robbiola et al [7] whom propose two kind of patina structures. Type I, mainly occurring at low corrosivity environments, has an "even" surface and a bilayer structure that is formed via internal Sn oxidation and selective Cu dissolution. Type II, occurring at highly corrosive conditions, often in the presence of chloride, has a "coarse" surface and a three-layer structure composed of a Sn-rich internal zone, a cuprous oxide layer and an external porous zone. The corrosion process is in the case of Type I controlled by the migration of Cu-cations through the patina, and for Type II by inward mass transport of negatively charged anions. The study concludes that the role of Sn on patina evolution is highly environmental dependent. Recent findings by the authors reveal that Sn-oxides with significant barrier properties are enriched within the native surface oxide and within the patina as a compact inner layer intercalated at the bulk alloy/patina interface of an aluminum-bronze alloy (Cu-5Zn-5Al-1Sn) [31,32]. Similar enrichment of Sn has been observed within the patina of a Cu4Sn bronze alloy [18,19] exposed at marine conditions [19]. The role of Sn on the oxidation, patina formation and evolution on Sn-bronzes is scarcely investigated.

Even though alloying of Cu with Sn generally results in a material of improved corrosion resistance (lower corrosion rate) [33], this behavior is not universal. Recent findings reported for marine conditions show similar, or even higher, corrosion rates of bronze (4 wt.% Sn) compared with Cu metal as well as patina flaking [18,19]. Recent field and laboratory findings show though that alloying with Sn does not largely alter the corrosion induced-release of copper from bronze (6 wt.%) compared to copper metal [34,35] at marine conditions. The reason is that the runoff process, that takes place at the interface between the patina and the environment, largely depends on the patina composition at the outermost surface, which at marine conditions predominantly is comprised of the same Cu-rich corrosion products as observed on Cu metal and that flaking takes place at both bronze and Cu metal at reported conditions [18,19]. The release of Sn was found negligible [34,36]. A thorough understanding of runoff mechanisms of Cu from naturally patinated Cu metal at different atmospheric conditions and the importance of environmental, climatic and surface conditions on the runoff process has during the last decades been elaborated by some of the authors [33,37]. Knowledge has also been gained for brass (Cu-Zn alloys) [19,38] and aluminum-copper alloys [19,32], whereas the knowledge on bronze is less explored and understood [34,36].

From an increased use of Sn-bronzes in architecture follows a need for scientifically based overall knowledge on their atmospheric corrosion and metal release performance. Such information is crucial from both an environmental and regulatory perspective. The main objective of this study is therefore to discern the role of Sn on the atmospheric corrosion and metal release for binary bronze alloys, Cu4Sn (4 wt.% Sn) and Cu6Sn (6 wt.% Sn), commonly used in contemporary architecture compared with Cu metal in terms of alloy microstructure, native surface oxide composition, corrosion rate, patina evolution, surface appearance and metal release rates, highlighting differences between urban and marine sites. Selected data will be presented based on multi-analytical investigations using complementary microscopic, spectroscopic, electrochemical and chemical tools, from several long-term (up to 5 years) non-sheltered field exposures of Sn-bronzes and Cu metal at two marine sites (Brest-France, Cadiz-Spain) and three urban sites (Milan-Italy, Madrid-Spain, Stockholm-Sweden) in Europe.

2. Experimental

2.1. Materials and surface preparation

The investigations were performed on commercially available bronze alloys, Cu4Sn (96 wt.% Cu, 4 wt.% Sn ≈ 2.2 at.% Sn), Cu6Sn (94 wt.% Cu, 6 wt.% Sn ≈ 3.3 at.% Sn) and copper metal (DHP-Cu, purity 99.98 wt.%), kindly provided via the European Copper Institute, Belgium.

Initial oxidation studies were performed on diamond polished coupons (2 × 2 cm^2) prepared according to the following procedure: mechanical grinding to 2400 grit, successive polishing to 0.1 µm, ultrasonic cleaning in ethanol (analytical grade ethanol, 10 min) and drying (cold nitrogen gas). All studies were conducted within 3 min after the sample preparation.

The field exposures were performed on as-received surfaces (ultrasonically degreased in acetone followed by isopropylic alcohol). More experimental details in Ref [18]. Cross-sections of exposed coupons were prepared by the embedment in a conductive polymer and stepwise polishing (0.25 µm diamond paste followed by OP-S suspension) (Struers A/S, Denmark) to near-mirror like surfaces.

2.2. Exposure conditions

The field exposure was conducted as described in the ISO 9226 [39] and the ISO 17752 standard [40] for corrosion rate and runoff rate studies, respectively. Coupons of bronzes and Cu metal were exposed (45° from the horizontal, facing south) at different marine (Sites 1, 2, 3,

Exposure sites	T (°C)	RH%	Amount of rain (mm y^{-1})
Milan	14 ± 6	59 ±18	600–1100
Madrid	17 ± 11	52 ± 24	200–400
Cadiz	19 ± 5	71 ± 15	300–600
Stockholm	8 ± 7	71 ± 17	450–650
Brest	13	82	800–1100

Fig. 1. Location of the urban (Milan, France; Madrid, Spain; Stockholm, Sweden) and the marine (Brest, France; Cadiz, Spain) test sites in Europe and average levels in temperature, relative humidity and annual rainfall quantity during the exposure periods. * 100 km from the seashore.

4* in Brest, France, Cadiz, Spain) and urban (Milan, Italy; Madrid, Spain, Stockholm, Sweden) test sites up to 5 years, Fig. 1. Detailed environmental information is given elsewhere (Brest [18,19]; Stockholm, Madrid and Milan [38]). The site of Cadiz, Spain, located approx. 1 km from the sea-shore, is characterized by similar deposition rates of chlorides (estimated, based on ion chromatography measurements of the runoff water from blank surfaces) as for site 2 in Brest, *i.e.* corrosivity class S_2 (S_2: 60–300 mg Cl^- m^{-2} d^{-1}) and the site of highest average temperature and a high relative humidity. Low SO_2 levels (< 10 µgm^{-3}) are characteristic for all sites with the highest levels in Madrid and Cadiz, and the lowest in Stockholm (< 1 µg m^{-3}).

2.3. Corrosion rates, metal release and surface appearance measurements

Corrosion rates were determined by repeated pickling of exposed coupons in amidosulfonic acid following the procedure described in ref [37]. Successful removal of corrosion products was ensured for both Cu metal and the bronzes using SEM/EDS analysis. Quantification of total concentrations of released Cu and Sn in runoff water samples continuously collected during the exposure periods was performed using AAS (atomic absorption spectroscopy) by means of a Perkin Elmer AAnalyst 800 instrument operated at standard conditions with limits of detection of 6 µg Cu L^{-1} (flame mode) and 2 µg Sn L^{-1} (graphite furnace). Detailed analytical procedure given in Refs [19,41].

Quantification of changes in surface appearance with time was evaluated by using spectrocolorimetry (Minolta CM2500D spectrophotometer) on 10 measurements for each coupon using D65 light. Relative changes in appearance are described according to the three-coordinate CIELab color reference space (a* (red/magenta-green), b* (yellow/blue) and L* (lightness - black to white)). Further details are given in Ref [32].

2.4. Microstructure and morphology characterizations

The microstructure of the alloy matrix was characterized by mean of electron backscatter diffraction (EBSD) at 20 kV accelerating voltage with a step size of 150 nm using a field emission scanning electron microscope (FESEM) equipped with an Oxford HKL Fast electron backscatter diffraction detector. Post-processing was carried out using the HKL CHANNEL5 software. Top surface- and cross-sectional morphologies of corrosion products were documented by means of scanning electron microscopy (SEM) using a LEO 1530 instrument with a Gemini column, upgraded to a Zeiss Supra 55 (equivalent). The images were recorded using a backscattered electron (BSE) detector at an accelerating voltage of 15 kV.

2.5. Surface oxide and patina compositional analyses

Auger electron spectroscopy (AES) and X-ray photoelectron spectroscopy (XPS) measurements were performed to assess elemental information of the outmost surface of freshly diamond polished, as-received and field exposed coupons of Cu4Sn and Cu6Sn. A PHI 710 Scanning Auger Microscope (ULVAC-PHI, Japan) was operated using an Ar^+ ion gun voltage of 10 kV and an electron incidence angle of 30° for the AES set-up. The chamber vacuum was maintained below 3.9×10^{-9} Torr. The lateral elemental distribution of the bulk matrix was determined by means of scanning Auger microscopy (SAM), and the spatial drift during scanning was calibrated using a SEM image. Spectra and images were post-processed using the PHI MultiPak software. A Kratos AXIS UltraDLD X-ray photoelectron spectrometer (Kratos Analytical, Manchester, UK) with a monochromatic Al X-ray source were used for the XPS measurements. Analyses were performed on different areas (between 2 and 6 different locations), approximately sized 700×300 µm^2, collecting overview spectra and high resolution spectra (20 eV) of C 1 s, O 1 s, Cu 2p, Cu KLL, and Sn 3d. The C 1 s peak position at 285.0 eV was used for binding energy calibration.

Information on elemental depth distribution within the patina was provided by means of glow discharge optical emission spectroscopy (GDOES, Leco GDS 850 instrument) combined with elemental analysis (line-, spot- and image-analysis) using energy dispersive spectroscopy (EDS, X-Max SDD, Silicon Drift 50 mm^2 detector, Oxford Instruments). The GDOES measurements, analyzed by the LECO data handling system, reflect information from a circular area (ϕ 4 mm) being continuously sputtered using Ar plasma at a pressure of 6–7.5 Torr, a potential of 700 V and a current of 20 mA to keep the sputtering rate constant. This technique has been shown an adequate detection ability to obtain a sufficient depth resolution with the corresponding chemical variations within thin films and to acquire quantitative information from the elements involved [42]. Calibration was conducted on a steel sample having an approximately 8 µm thick oxide composed of 27.5 wt.% oxygen.

The lateral distribution of functional groups within the patina was determined by means of confocal Raman micro-spectroscopy (CRM) with a WITec alpha300 system with a laser source with a wavelength of 532 nm A lateral resolution of approximately 300–400 nm was managed via a Nikon NA0.9 NGC objective. Functional groups within the patina were identified by means if IRAS (infrared reflection absorption spectroscopy, Digilab 4.0 Pro FTIR spectrometer) using a MCT detector (4000–400 cm^{-1}) collecting 1024 scans with a resolution of 4 cm^{-1}. The spectra are presented in absorbance units ($-\log (R/R_0)$), where R is the reflectance of the exposed coupon and R_0 the reflectance of a non-exposed surface, *i.e.* a freshly polished Cu metal coupon [43].

Crystalline patina constituents of stripped corrosion products were identified by XRD (X-ray diffraction) and GIXRD (grazing incidence X-ray diffraction) at the top-surface of exposed coupons using an X'pert PRO PANALYTICAL system, equipped with an X-ray mirror (CuKα radiation) and a 0.27° parallel plate collimator. GIXRD data was generated using an incidence angle of 1° and 2° (corresponding to an approximate surface penetration depth of 0.4–1.0 µm).

The influence of Sn on the reduction/oxidation processes of the Cu4Sn alloy compared with Cu metal was assessed by means of cyclic voltammetry (CV) using a PARSTAT multichannel PMC Chassis instrument equipped with six PMC-1000 (AC/DC) channels, an electrolyte of 0.1 mol L^{-1} KCl, a Ag/AgCl Ag(s)|AgCl(s)|Cl^- (aq, Saturated KCl) reference electrode, and a platinum mesh as counter electrode. Oxygen-free conditions were achieved by purging the solution with N_2 gas 30 min before the start of the experiments. Voltammograms were acquired from 0.0 V to −1.3 V to 0.0 V (*vs.* Ag/AgCl) using a scan rate of 20 mV s^{-1}.

3. Results and discussion

In the following, the influence of Sn on the microstructure and native surface composition of Sn-bronzes (4, 6 wt.% Sn) is highlighted and compared with Cu metal in terms of their corrosion performance, patina evolution and release of Cu and Sn on a long-term (up to 5 years) perspective at different urban and marine outdoor conditions. All field exposures were performed on as-received (non-polished) surfaces of Cu4Sn/Cu6Sn to mimic realistic conditions for their use in architecture.

3.1. Alloying with Sn results in a microstructure of reduced grain size and an increased fraction of twin boundaries compared with Cu metal but does not result in any segregation at either grain boundaries or in grains

As similar results were obtained for Cu4Sn and Cu6Sn, only data for Cu4Sn will be presented below. Similar to Cu metal, the Cu4Sn alloy forms a single phase of face centered cubic (fcc) solid solution. A major inherent difference between Sn-bronze and Cu metal is that alloying with Sn can result in microstructural differences such as grain boundary segregation, secondary phases and the introduction of residual stresses, as well as local variations in chemical composition, characteristics that may influence the corrosion behavior [33]. The microstructure and the

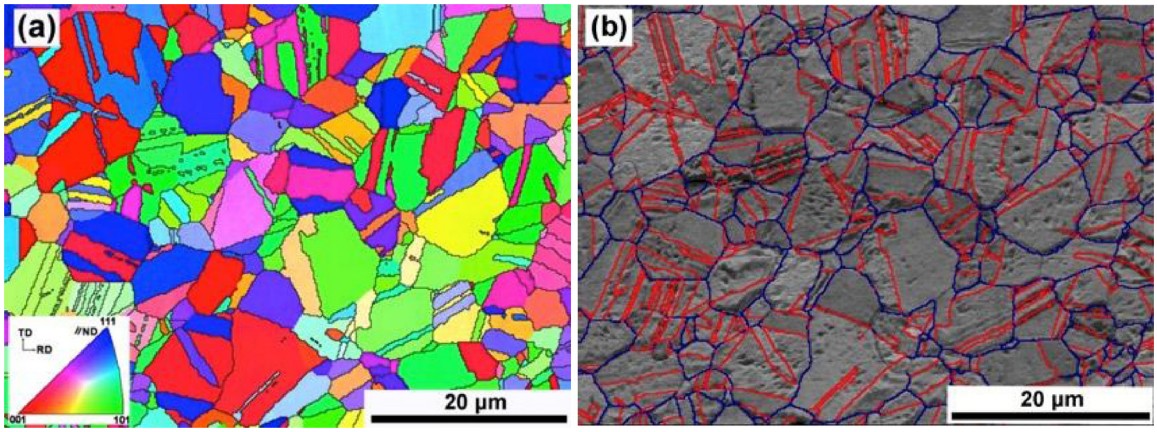

Fig. 2. EBSD grain color map (a) and image quality map (b) of the Cu4Sn bulk material displaying different type of grain boundaries (random high angle boundaries (misorientation > 15°), in blue). Twin boundaries (Σ3, a common crystal plane along which two crystals form a mirror-symmetric orientation relationship) are indicated in red (For interpretation of the references to colour in this figure legend, the reader is referred to the web version of this article.).

chemical composition of the bulk material were therefore analyzed by means of EBSD and scanning-AES.

The microstructure of Cu4Sn in terms of grain orientation, grain size and grain boundaries are presented in the EBSD images of Fig. 2a and b. The statistical analysis of the grain size, Fig. 2a, shows an average grain size diameter being 7–8 times smaller (1.4 µm) compared with corresponding grains of microcrystalline DHP-Cu metal (10.4 µm) [31]. The blue and red lines in Fig. 2b, indicate random high angle boundaries (misorientation > 15°) and twin boundaries (a common crystal plane along which two crystals form a mirror-symmetric orientation relationship, *i.e.* a specific orientation relationship), respectively. Statistical analysis shows a fraction of twin boundaries of 44% for the Cu4Sn alloy, which is almost three times higher than for Cu metal (16%), reported in Ref [31]. The results suggest improved mechanical properties of Cu4Sn as twin boundaries act as strengthening phases that efficiently block dislocation motions during plastic deformation [44].

In order to investigate possible compositional variations in a qualitative manner within the Cu4Sn substrate, Ar^+-ion sputtering was performed to a depth of ≥ 20 nm into the bulk alloy on a freshly diamond-polished surface. The top-surface (by means of SEM) after sputtering is displayed in Fig. 3a with individual grains observed due to selective etching during the sputtering process. The corresponding SAM image of Sn for Cu4Sn is shown in Fig. 3b. No significant segregations of Sn between different grains or between grains and adjacent grain boundaries were observed. Similar findings were obtained for Cu6Sn (data not shown).

In all, the Cu4Sn bulk alloy reveals no significant lateral variation in microstructure or chemical composition. Compared with Cu metal, examined in Ref [31], Cu4Sn exhibits a smaller grain size and a larger fraction of coherent twin boundaries, beneficial from both a mechanical and corrosion perspective.

3.2. Alloying with Sn results in the formation of an approximately 1 nm thick native surface oxide that predominantly consists of Cu_2O and Sn-oxides. Surface enrichment of Sn improves the barrier properties (corrosion resistance) of the oxide

Elemental AES depth distributions (shown down to a sputtering depth of 5 nm) of Sn, Cu and O obtained from the diamond polished surfaces are presented in Fig. 4a. Judged from the O-profile, most of the oxide has been removed at a depth of approximately 1 nm at which the profiles of Sn and Cu have reached relatively constant levels, largely corresponding to their individual bulk contents. The enrichment of Sn within the oxide is evident for both Cu4Sn, Fig. 4a, and for Cu6Sn, Fig. 4b. A somewhat larger enrichment of Sn within the native oxide of Cu6Sn compared with Cu4Sn reflects the slightly higher Sn bulk content (indicated by the dotted lines in each figure). The results are consistent with XPS findings showing an oxidized Sn to oxidized Sn + Cu mass ratio of 0.08 ± 0.01 for Cu4Sn and 0.10 ± 0.01 for Cu6Sn, *i.e.* slightly higher for Cu6Sn. Binding energies of the Cu $2p_{3/2}$ peak at 932.7 ± 0.1 eV with a minor contribution (< 5%) of metallic Cu (Auger peak) for both alloys predominantly reflect the presence of Cu(I)

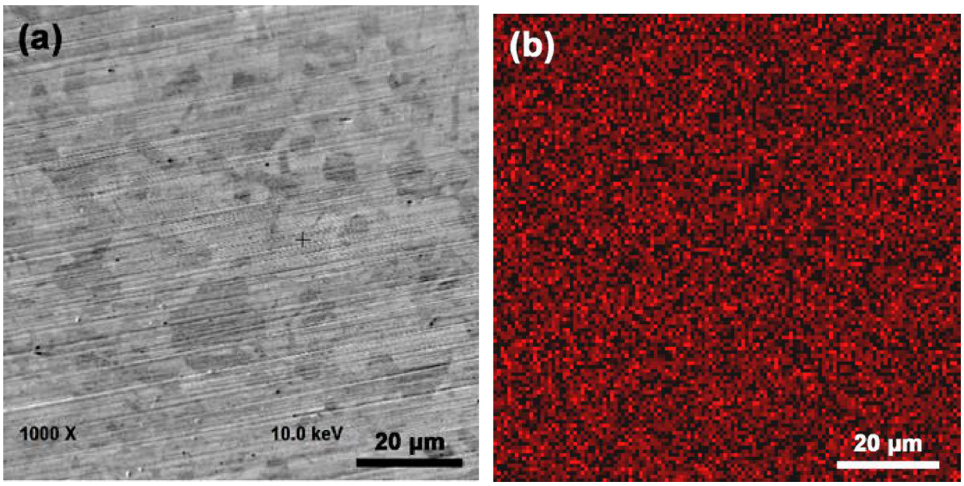

Fig. 3. SEM image of the Cu4Sn surface after sputtering into the bulk material (a) and corresponding SAM image of the elemental distribution of Sn (b).

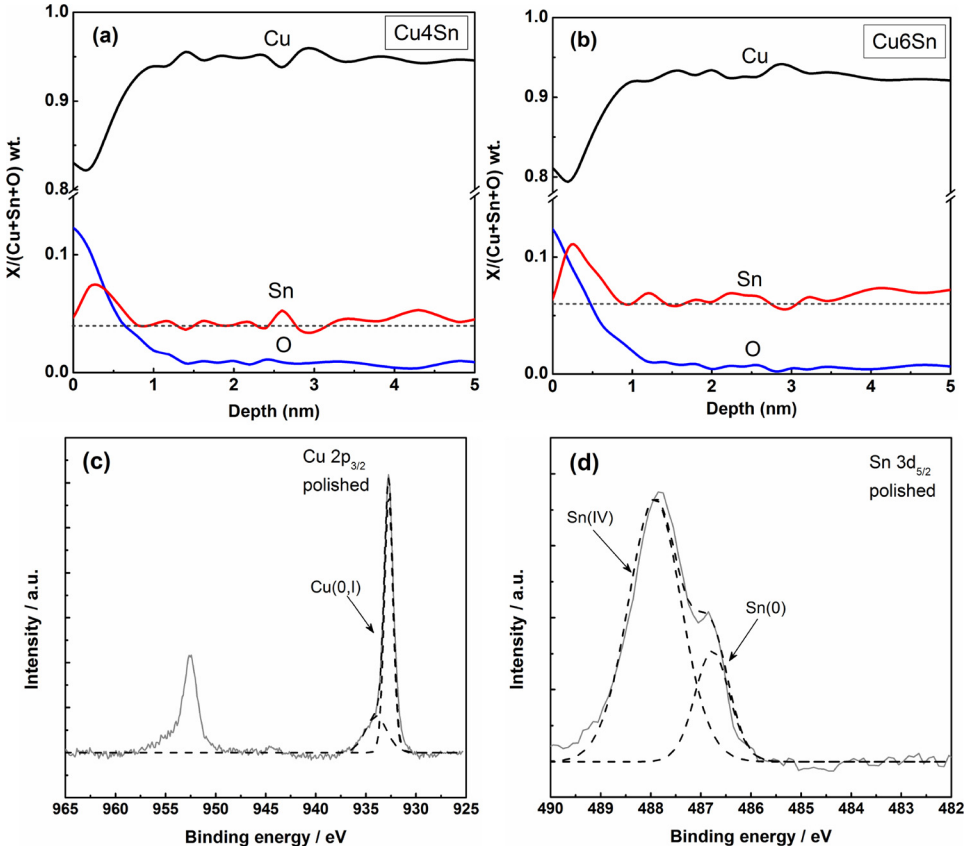

Fig. 4. Depth profile analysis (wt.%) by means of AES of the native oxide spontaneously formed on freshly diamond polished Cu4Sn (a)* and Cu6Sn (b), and XPS spectra of the $Cu2p_{3/2}$ and the Sn $3d_{5/2}$ peaks for freshly polished Cu4Sn (c). * Measurements made on duplicate coupons.

surface species. A Sn $3d_{5/2}$ peak position at 487.8 ± 0.2 eV implies the possible presence of SnO_2 (and/or possibly SnO), Fig. 4c. Metallic Cu and Sn signals confirm the thin oxide thicknesses observed by means of AES.

Cyclic voltammograms of Cu metal and Cu4Sn were acquired immediately after diamond polishing to discern the influence of Sn on the initial oxidation of Cu4Sn, Fig. 5. Emphasis was placed on the nature of the native surface oxides and not on their electrochemical behavior at immersion conditions. The cathodic scan of Cu metal with its native surface oxide shows a cathodic peak at −0.75 V, which is attributed to the reduction of Cu_2O to Cu, the reduction of a precursor (previously assigned as Cu_xO with mixed valence states between Cu and Cu(I)), to Cu at potential between −0.55 to −0.65 V, and/or possibly to some extent to the reduction of CuO to Cu at −0.55 V [14,45,46]. The increased current after the sweep to −1.15 V is associated with hydrogen evolution [31,45]. The anodic peak observed at −0.22 V corresponds to the oxidation of Cu to Cu(I), which probably relates to the formation of CuCl [15,47,48]. In contrast, the cathodic reduction peak, corresponding to Cu_2O initially present on Cu4Sn, occurred at a lower potential (−0.88 V) compared with Cu metal (−0.75 V). This potential shift is attributed to the intercalation of Sn-oxides in the outermost surface oxide. The minor cathodic peak observed at approximately −0.60 V may be related to the reduction of Cu_xO and/or CuO. Observed blocking effects of Sn-oxides within a Cu-rich surface oxide are consistent with findings for Sn-bronzes at immersion conditions [14,17,49]. Similar findings have also been observed for an aluminum-bronze alloy (Cu-5Zn-5Al-1Sn) [31,32]. The anodic peak at −0.65 V is related to the transformation of Sn(0) to Sn(II), or Sn(II) to Sn(IV), and the peak at −0.14 V to the possible formation of CuCl [14,49]. The latter peak is slightly shifted compared with observations for Cu metal (−0.22 V), and attributed to the presence and intercalation of Sn-containing compounds that suppress the oxidation of Cu at the Cu4Sn surface [15].

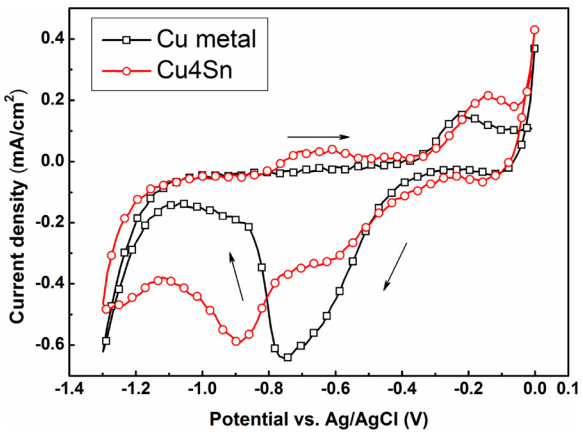

Fig. 5. Cyclic voltammograms of freshly diamond polished Cu metal (a) and Cu4Sn (b) in oxygen-free 0.1 mol L^{-1} KCl.

Since the polished surface state is not a surface for architectural use, the as-received (aged) non-exposed surface of the Cu4Sn alloy was examined using GDOES, Fig. 6. Similar to the freshly polished surface, the enrichment of Sn was evident within the surface oxide being 5 times higher compared with the polished surface and 5–50 times enriched compared with the bulk alloy composition, see Fig. 6b. The approximate thickness of the as-received surface oxide was estimated to 5–10 nm, *i.e.* 5–10 times thicker than the oxide spontaneously formed on the freshly polished surface, Fig. 4a. Similar findings were observed for an as-received surface of Cu4Sn by means of XPS showing a much more oxidized surface consisting of Cu(I)-, Cu(II)- and Sn(IV)- (probably SnO_2 and/or SnO) oxides, Fig. 6c and d. The Sn content of the as-

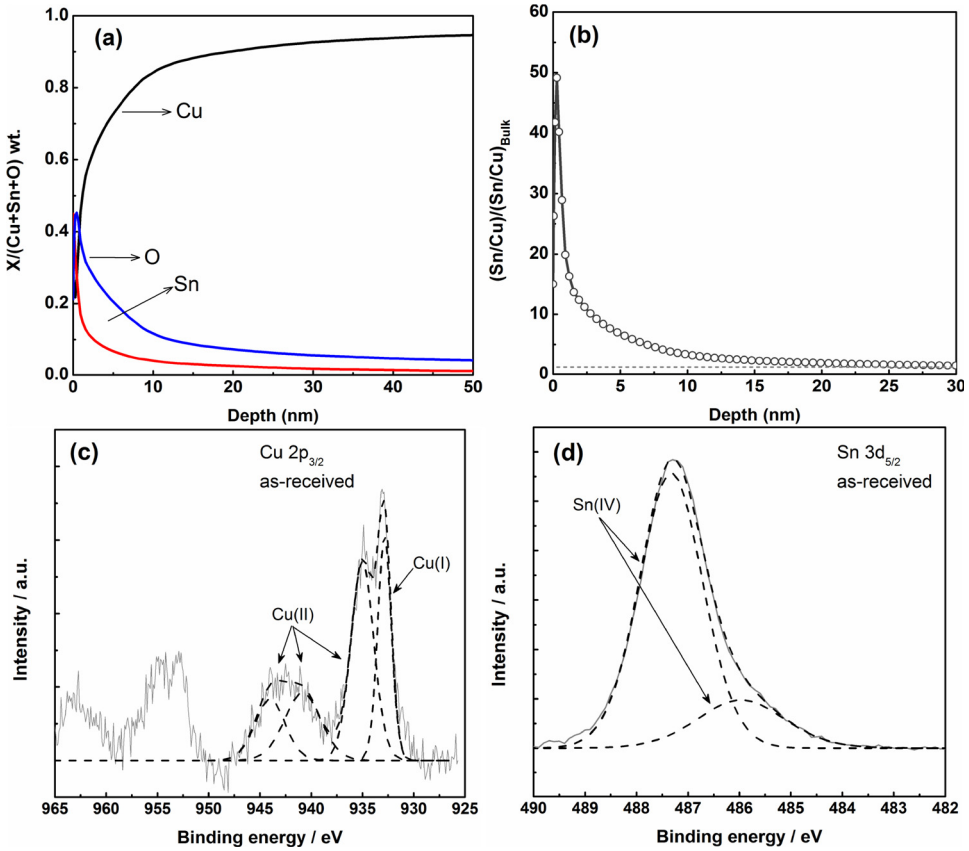

Fig. 6. Depth profile analysis (wt.%) by means of GDOES (a) and the relative distribution of Sn compared with Cu compared with their bulk contents (b), and XPS spectra of Cu2p (c), and Sn3d$_{5/2}$ (d) for unexposed as-received Cu4Sn.

received surface oxide (not the same coupon as for the GDOES measurement) was approximately 5 times higher and the oxide significantly thicker (no metallic Cu signal in the Auger peak observed for any of the alloys) compared with freshly polished conditions. Similar results were obtained for Cu6Sn (data not shown). The results clearly show the importance of material history and storage prior to use, and that Sn-bronzes spontaneously form a surface oxide containing Sn oxides.

In all, the combined information from AES, GDOES, XPS and CV measurements shows that a freshly polished Cu4Sn alloy spontaneously forms an approximately 1 nm thin surface oxide primarily composed of predominantly Cu_2O and Sn-oxides, where the latter induces blocking properties on Cu oxidation and Cu-oxide reduction. A non-exposed as-received surface of the Cu4Sn alloy is at least 5–10 times thicker and shows an even higher enrichment of Sn in the surface oxide compared with a freshly polished surface and compared with the bulk composition.

3.3. Alloying with Sn results in reduced corrosion rates and thinner patinas compared with Cu metal in low-chloride containing urban environments but similar or even higher corrosion rates and thicker patinas at chloride-rich marine conditions

The importance of the native Sn-rich surface oxide and its evolution on Sn-bronzes (Cu4Sn/Cu6Sn) compared with the surface oxide of Cu metal on the corrosion performance is evident from the field exposure results. Annual corrosion rates, determined after one year of exposure (a typical time-frame for site corrosivity measurements [39]) and after a longer time periods (three or four years), clearly show different trends with lower corrosion rates (2–7 times) of the Sn-bronzes compared with Cu metal at the urban sites (Fig. 7a), whereas the corrosion rates are similar or even higher (due to the patina characteristics as described in Section 3.4) for the alloys exposed at the marine sites, Fig. 7b. Observed corrosion rates are significantly (5 to 10 times) lower at the urban sites compared with the marine sites. At marine conditions, the corrosion rates are strongly reduced as a function of distance from the sea-shore, for both Cu metal and the Sn-bronzes as illustrated for the three sites in Brest of reduced chloride content in air (Site 1-corrosivity class S_3: 300–1500 mg m^{-2} d^{-1}, Site 2-S_2: 60–300 mg m^{-2} d^{-1}, Site 3-higher range of S_1: 3–60 mg m^{-2} d^{-1}, Site 4: lower range of class S_1: 3–60 mg m^{-2} d^{-1} [18]). With respect to chloride deposition, the conditions in Cadiz (~20 mg m^{-2} d^{-1}) are similar to site 4.

The corrosion rates at the urban sites were 2–3 and 2–10 times lower for the Cu4Sn and Cu6Sn alloys than observed for the Cu metal, respectively, indicative of different corrosion mechanisms and kinetics compared with marine conditions. The highest first-year corrosion rates were observed for Cu4Sn exposed in Stockholm followed by Milan and Madrid, despite lowest pollutant levels of *e.g.* SO_2 (Stockholm: 2 ± 1 μg m^{-3} < Milan: 6 ± 5 μg m^{-3} < Madrid: 10 ± 5 μg m^{-3}). This is attributed to differences in climatic conditions between the sites [19,38] in terms of cyclic wet-dry conditions, rainfall characteristics and frequency, temperature and RH rather than to differences in environmental pollutant levels and chloride deposition rates, aspects previously discussed for Cu metal [37] and different Cu-based alloys [38].

Reduced corrosion rates of Sn-bronzes compared with Cu metal at the urban sites of low chloride-levels are consistent with literature findings [19,22,50]. As an example, findings from a large international field exposure program of different construction materials exposed for different time periods in 20 different urban sites of Europe reported on average 25% lower first-year corrosion rates of a cast bronze alloy compared with Cu metal during the period 1987–1995, and 45% lower levels during 1997–2001 [20]. The results clearly elucidate the importance of the native Sn-rich surface oxide for the corrosion performance of Sn-bronzes at urban conditions whereas its beneficial effects

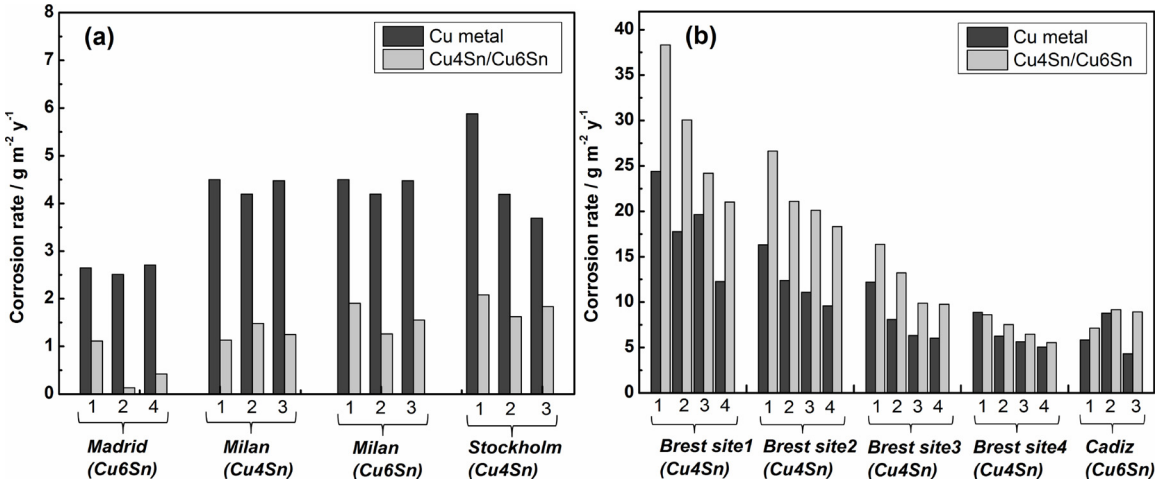

Fig. 7. Average annual corrosion rates of Cu metal, Cu4Sn and/or Cu6Sn exposed after 1–4 years at different urban (a) and marine (b) sites.

on the corrosion rate of Cu4Sn compared with Cu metal is not obtained at chloride-rich marine sites, Fig. 7b.

In all, alloying with Sn results in a Sn-rich native surface oxide that improves the corrosion performance compared to Cu metal at urban conditions via a slow patina growth. No beneficial effects were observed at marine conditions in which the patina growth is much more rapid. Observed differences in corrosion rates between Cu metal and Cu4Sn/Cu6Sn result in patinas of different thickness being thinner for the alloy at the urban sites, and similar and even thicker at the marine sites, see Fig. 8. Differences in patina morphology and composition are discussed in Section 3.4.

3.4. Alloying with Sn results in differences in patina morphology and distribution of Cu- and Sn-rich corrosion products at low-chloride containing urban conditions compared to marine chloride-rich environments

A multitude of analytical techniques were employed to identify corrosion products within the patinas formed at the different test sites after 1–5 years of exposure with the aim to elucidate the role of Sn on the patina evolution of the Sn bronzes.

In agreement with frequent literature findings [4,7,13,18,19,23], all patinas observed for Sn-bronzes consist of the same corrosion products as observed for Cu metal, and are predominantly composed of different copper-rich crystalline corrosion products including cuprite (Cu_2O), posnjakite ($Cu_4SO_4(OH)_6{\cdot}H_2O$), and brochantite ($Cu_4SO_4(OH)_6$) at the urban sites, and of Cu_2O, nantokite (CuCl), and paratacamite/atacamite ($Cu_2(OH)_3Cl$) at the marine sites. The non-crystalline nature and the wavenumber cutoff for Sn-oxides and their partial overlap with peaks of Cu_2O disabled their possibility to be unambiguously identified using XRD and FTIR/IRAS, respectively, see Supporting information. The presence and elemental distribution of Sn within the patinas are therefore in the following predominantly elucidated using findings of XPS, GDOES and EDS. Confocal Raman measurements were performed on the marine formed patina.

Different Sn-oxides including SnO_2, SnO and hydrated $SnO_2{\cdot}nH_2O$ have been suggested in the literature as non-crystalline patina constituents of Sn bronzes [7] and on Sn metal [51] exposed at atmospheric conditions. The presence of Sn-oxides within the patinas was evident for all sites in this study being present in the inner part of the patina and/or evenly distributed within the patina at the urban sites, as illustrated for the urban sites (*e.g.* Milan and Madrid) in Fig. 9a-b. Patinas with stratified Sn-rich layers were typical for the marine sites, here illustrated with Cu6Sn exposed in Cadiz and Cu4Sn exposed at Brest site 1, Fig. 9c-d. This patina morphology with Sn-rich streaks was even more pronounced at conditions of higher deposition rates of chlorides as elucidated with the elemental mapping of Cu, Sn, O and Cl for Cu6Sn after 5 years in Brest (site 1), Fig. 10. The figure clearly illustrates Sn-rich streaks and a predominance of Cl-rich corrosion products at the outermost surface (identified as $Cu_2(OH)_3Cl$, see Figs. 10 and 11b). Cl-rich corrosion products exist also to a minor presence at the bulk-patina interphase and in streaks within the patina. This is, as described earlier, related to the formation and transformation of CuCl into $Cu_2(OH)_3Cl$ and the concomitant patina flaking taking place at the marine site and caused by its volume expansion [18,28]. Systematic laboratory investigations are on-going by the authors to mechanistically elucidate the effect that the Sn-rich corrosion products have on the corrosion rate, Fig. 7b, at chloride-rich conditions. No flaking of the patina was consistently taking place at the urban sites. Combined CRM mapping imaging on a segment of the streaked patina is illustrated in Fig. 11. In addition to the predominating presence of Cu_2O (in blue) with main peaks at 219, 424 and 636 cm^{-1} [52] and $Cu_2(OH)_3Cl$ (in yellow) with main peaks at 373, 519, 930, 977, 3364 and 3447 cm^{-1} [53] within the patina [18], the poorly adherent patina is dominated by the presence of CuCl (in green) with main peaks at 290, 613 and 1110 cm^{-1} [18]. These findings support previous observations and conclusions on the role of CuCl on the flaking process [18] and are consistent with SEM cross-sectional findings, Figs. 8 and 9. CRM findings elucidate furthermore the intercalation of SnO_2 (in red) within the Cu_2O-rich patina, in particular at the bulk/patina interface. The presence of SnO_2 was assigned based on its main peak at 632 cm^{-1} [54], though overlapped with the secondary peak of Cu_2O in the region of 630–640 cm^{-1} (Fig. 11c-d). CRM findings are in line with the results of AES (Fig. 4), GDOES (Figs. 6 and 12) and EDS (Figs. 9 and 10). Representative XRD data is given in Supporting information.

The lack of Sn at the outermost top surface at the marine sites was confirmed using both XPS (only Cu(II)-, oxygen- and chloride-containing corrosion products were observed at the outmost surface) and GDOES. The latter technique, Fig. 12a, showed a slightly depleted Sn content in relation to Cu in the outermost 2–3 μm of the top surface compared to the bulk content, and a significant enrichment of Sn within the streaked thick (30–35 μm) patina. As evident from the line scans of the urban patinas in Fig. 9a-b, Sn was present both in their inner and the outer parts. The enrichment of Sn (2–5 times) was also evident from the GDOES measurements in Fig. 12b, illustrated for patinas of Cu4Sn after 1 and 5 years of exposure in Stockholm and in Milan, respectively. The presence of Sn(IV) oxides at the outermost surfaces of the urban patinas was also observed by means of XPS showing $Sn_{ox}/Sn_{ox}+Cu_{ox}$ mass ratios of 0.048 ± 0.004 and 0.038 ± 0.002 after 1 and 5 years in Stockholm and 0.016 ± 0.002 and 0.062 ± 0.015 after 1 and 5 years in Milan.

In all, the patinas of Cu4Sn and Cu6Sn are predominantly composed of the same Cu-rich corrosion products as observed for Cu metal at

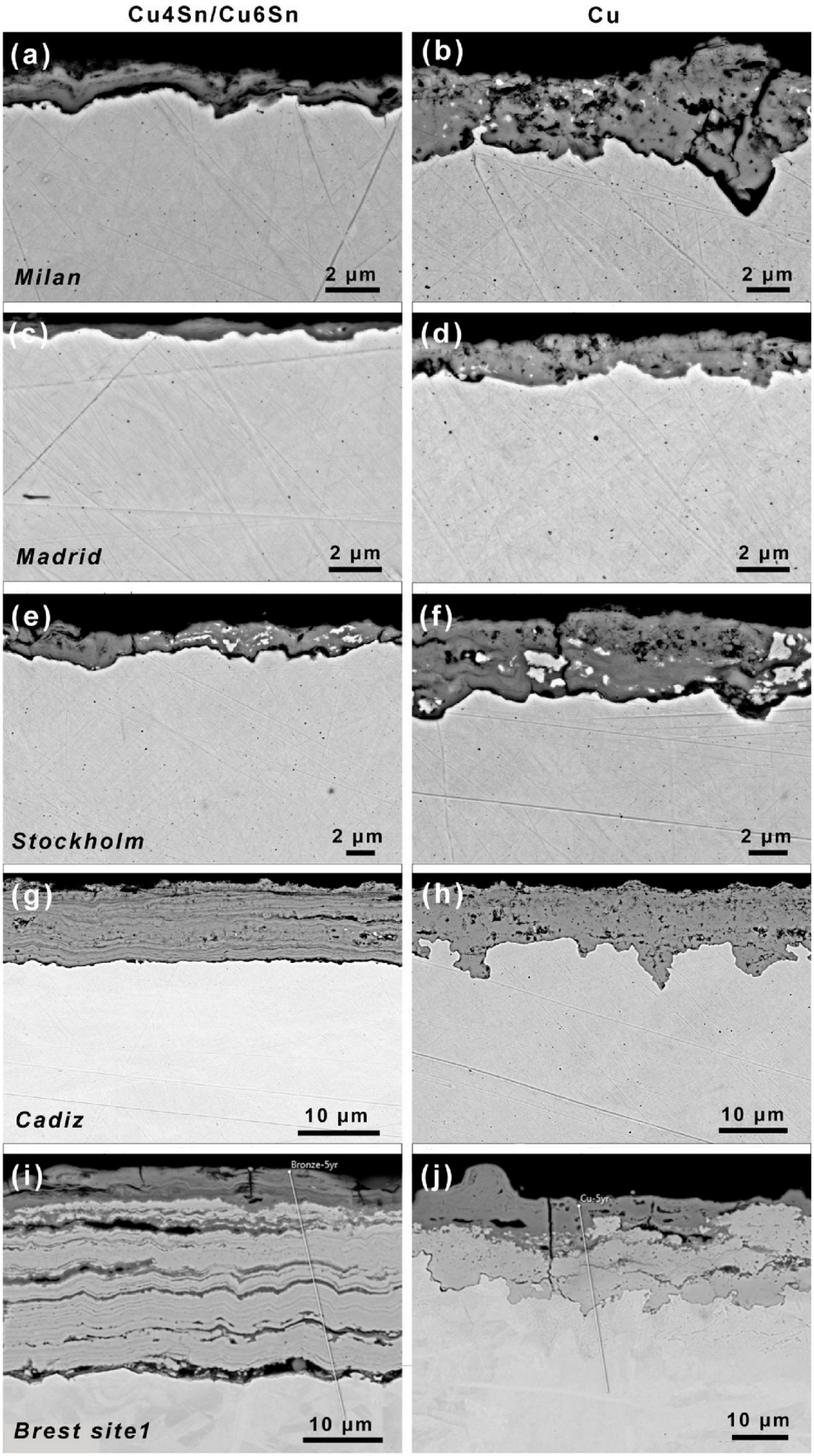

Fig. 8. Cross-sectional images of patina thickness and morphology of Cu4Sn/Cu6Sn (left) and Cu metal (right) exposed at urban (Milan-a, b, Madrid-c, d Stockholm-e, f) and marine sites (Cadiz-g, h and Brest site 1-i, j) for 4 or 5 years.

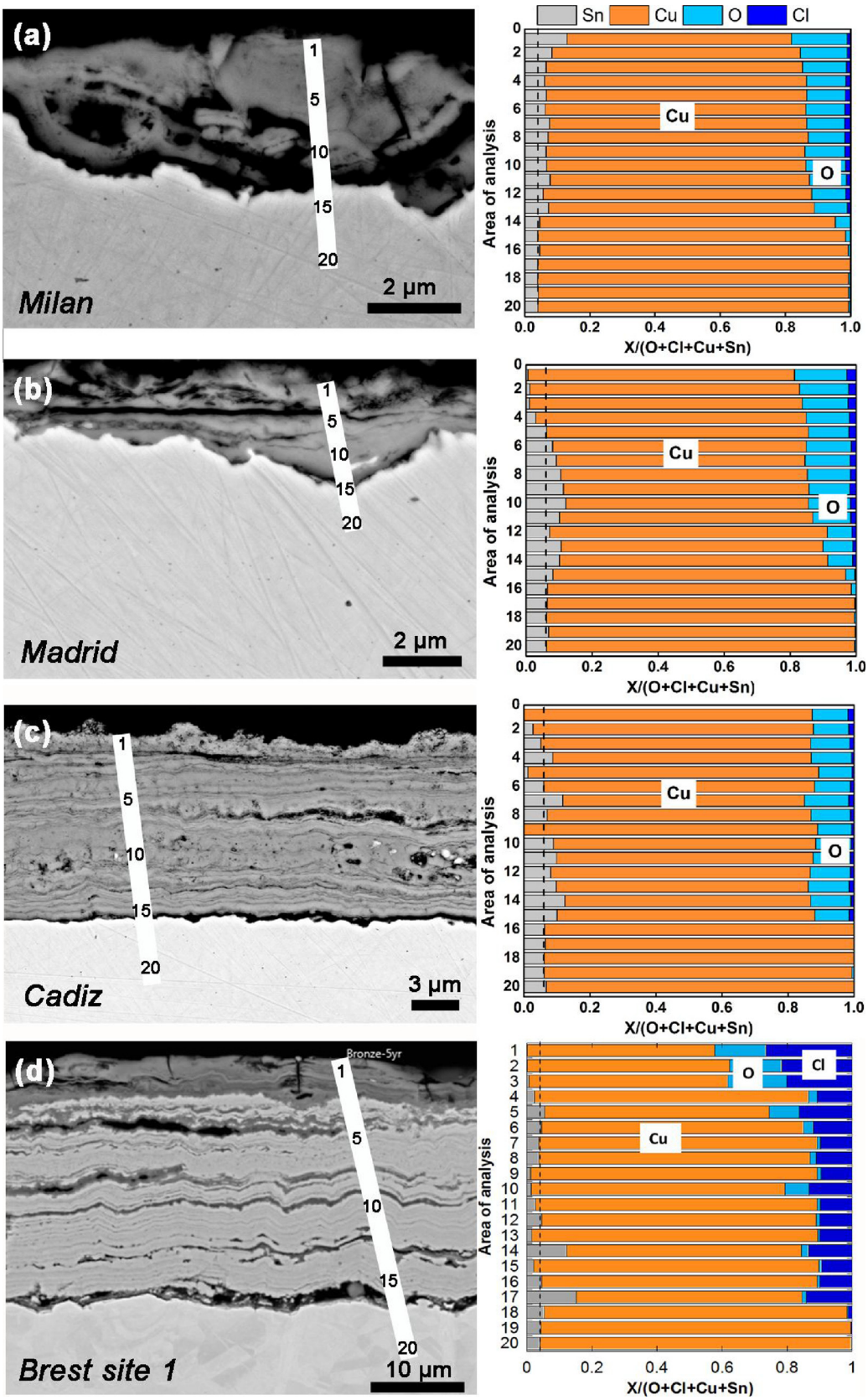

Fig. 9. SEM cross-sectional images (left) and corresponding relative elemental (wt.-%) distributions (right) of Cu, Sn, O and Cl within the bronze patinas after 4 or 5 years of exposure at urban conditions of Milan (a, Cu4Sn-5 year) and Madrid (b, Cu6Sn-4 year), marine conditions of Cadiz (c, Cu6Sn-4 year) and Brest site 1 (d, Cu4Sn-5 year). The dotted lines in the right figures indicate the Sn bulk content.

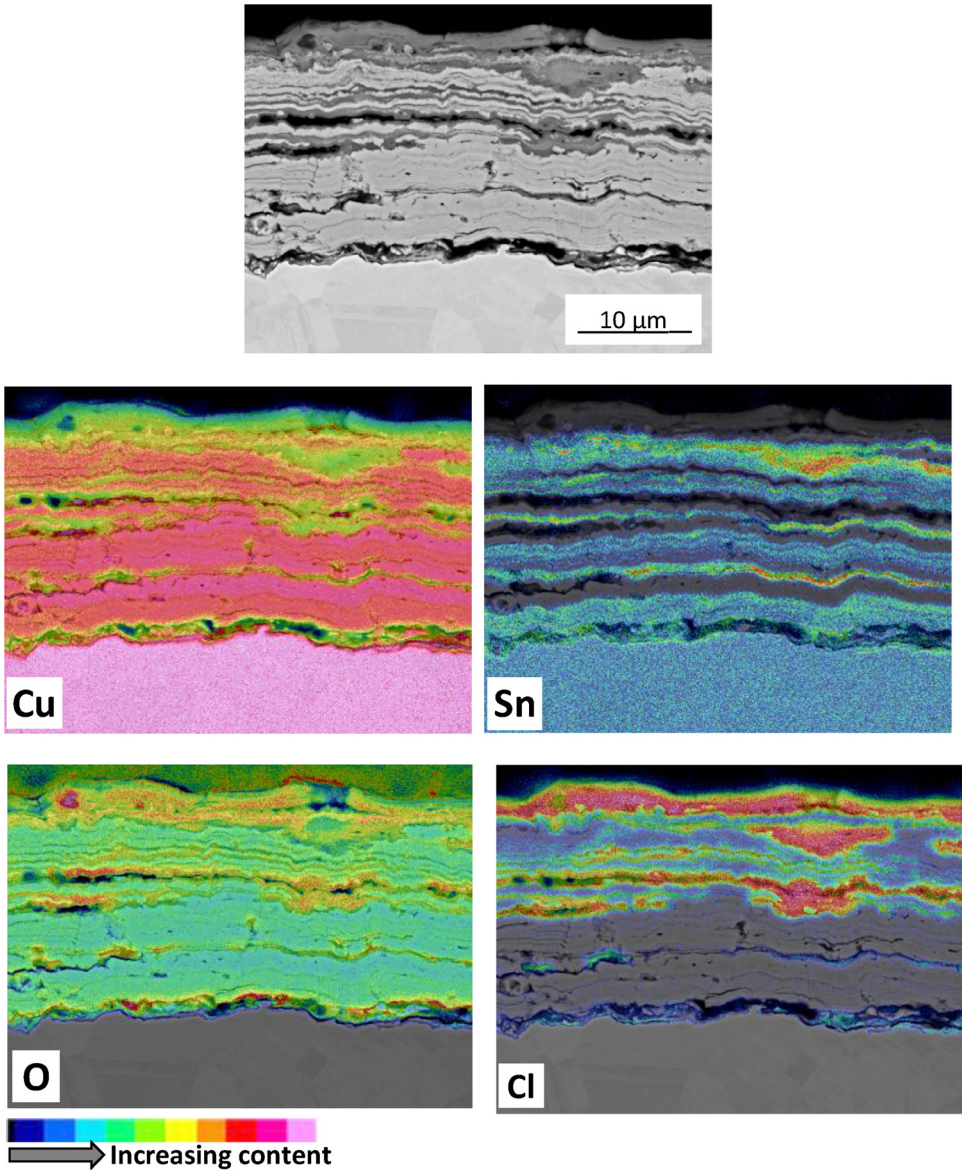

Fig. 10. SEM cross sectional image and elemental mapping of Cu, Sn, O and Cl in the patina of Cu4Sn exposed at non-sheltered marine (Brest site 1) for 5 years.

given exposure conditions. Sn-oxides (mainly SnO_2) are enriched to some extent within the entire patina at urban conditions whereas stratified layers with Sn-oxides form within the patina at marine conditions and do not act as efficient corrosion barriers.

3.5. Alloying with Sn influences the short-term surface appearance at urban conditions due to the slow formation rate of thin patinas whereas no significant effect is seen after long-term exposures at either urban or marine conditions

To visualize changes in surface appearance with time (patina evolution), optical stereomicroscopy imaging and spectrophotometric measurements were performed on all exposed samples, sites and time periods. Selected results (after 1 month, 1, 2 and 5 years) are presented in Fig. 13 compiled for the urban (a) and the marine sites (b).

The surface appearance of the Cu4Sn and Cu6Sn alloys at the urban sites becomes with time similar to the appearance of Cu metal in the red/yellow quadrant. However, as the corrosion rate is slower and the patina thickness thinner for the Sn bronzes at comparable time periods due to the presence of Sn-oxides, *c.f.* Figs. 2 and 3, the appearance is slightly shifted towards yellow as the lightness is higher compared with Cu metal. These differences in appearance are exemplified in Fig. 13a after 1 and 5 years of exposure in Madrid. The trend is though that the surface appearance of the Sn-bronze and Cu metal exposed at low-chloride containing urban conditions with time will coincide in both color coordinates and lightness. At the marine sites, Fig. 13b, a slight difference in lightness between the Sn bronzes and Cu metal, similar to findings for the urban sites, can be seen but otherwise very similar surface appearance, here illustrated with optical images from Brest site 1 after 1 and 5 years of exposure. This is consistent with the high and similar corrosion rates and formation of thick patinas predominantly composed of copper-rich corrosion products at the outermost surface for both Sn-bronze and Cu metal.

In all, due to the formation of the same Cu-rich corrosion products in the outermost patina on Cu4Sn/Cu6Sn and Cu metal exposed at the urban and the marine environments, no large differences in color coordinates are observed between the materials. Generally thinner patinas on the Sn bronzes compared to Cu metal at urban conditions result though in higher lightness values and hence a more yellowish appearance after short-term exposures. Minor differences were observed at marine conditions after short-term exposure. Similar appearances are expected after long-term exposures for Cu metal and Sn-bronzes.

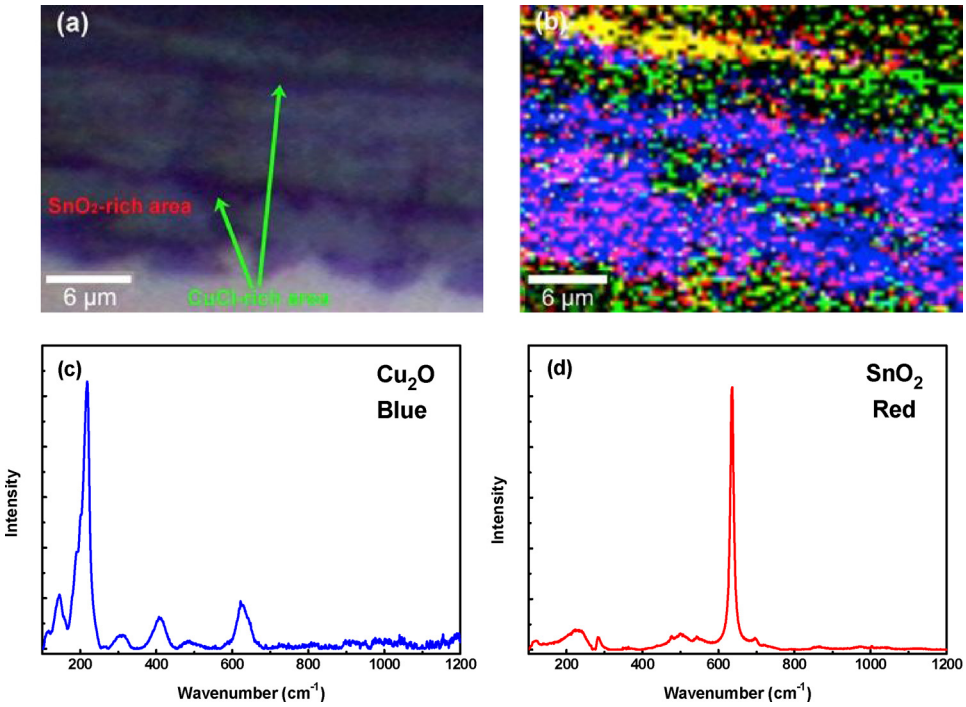

Fig. 11. Optical image (a) and combined CRM mapping image (b) of bands assigned to Cu_2O (blue, integrated between 150 and 250 cm^{-1}), SnO_2 (red, integrated between 600 and 700 cm^{-1}), CuCl (green, integrated between 250 and 350 cm^{-1}) and OH-groups (yellow, integrated between 3300 and 3500 cm^{-1}) in the 5 year old patina on Cu4Sn in Brest (site 1) (For interpretation of the references to colour in this figure legend, the reader is referred to the web version of this article.).

3.6. Alloying with Sn has a minor influence on the runoff rate of Cu from Sn bronzes, both at urban and at marine conditions. No Sn is released to the environment

In addition to prevailing environmental and climatic conditions as well as rainfall characteristics at given test sites, the constituents of the patina largely govern the extent of metal release at outdoor conditions [33,37,41,55]. In contrast to oxidation (corrosion) processes that at atmospheric conditions largely are controlled by electrochemical reactions at the patina/substrate interface, the runoff process is primarily governed by chemical reactions taking place at the interface between the patina and the atmosphere [33,41]. From this follows that most of the oxidized (corroded) metal forms adherent poorly soluble corrosion products and that only a fraction of oxidized metals within the patina is dissolved by repeated dry/wet cycles and corrosive constituents and released from the surface into the environment by the action of *e.g.* rain water. Long-term studies show significantly lower runoff rates of Cu compared to corresponding first-year corrosion rates for Cu metal and Cu alloys [29,32,44]. Similar observations were made in this study for all sites with runoff rates between 60%−95% (Madrid˜70%, Milan˜60%, Stockholm˜60%, Brest site 2˜95%, Cadiz˜93%) lower than the corresponding first-year corrosion rates.

Continuous monitoring of the total amount of released Cu and Sn from the Sn bronzes, exposed at 45° from the horizontal facing south, was performed at the urban (Stockholm, Madrid, Milan) and marine sites (Brest site 2, Cadiz) up to 5 years of exposure. The time dependence followed the same trends as previously described (data not shown) [19,32,35,36]. In order to enable the comparison between Cu4Sn/Cu6Sn and Cu metal at, and between the different sites, all annual runoff rates are normalized to the annual rainfall quantity of each site as the sites are characterized by large differences in rainfall quantities and the exposures have different starting periods, Fig. 14. No detectable amounts of released Sn were determined for any of the sampling periods (< 0.002 mg L^{-1}) or sites, which reflects poor-solubility of the Sn-oxides [56,57] at given conditions and their minor presence at the outermost surface as shown with XPS, GDOES and EDS, see 3.2. Compared with measured first-year corrosion rates, Fig. 7, total annual released amounts of Cu are for all sites lower during subsequent years, and no evident differences in release rates of Cu between Cu metal and the Sn-alloys are observed, neither at the urban (as observed for the corrosion rate) nor at the marine sites. These results indicate that differences in patina morphology within the patina and the

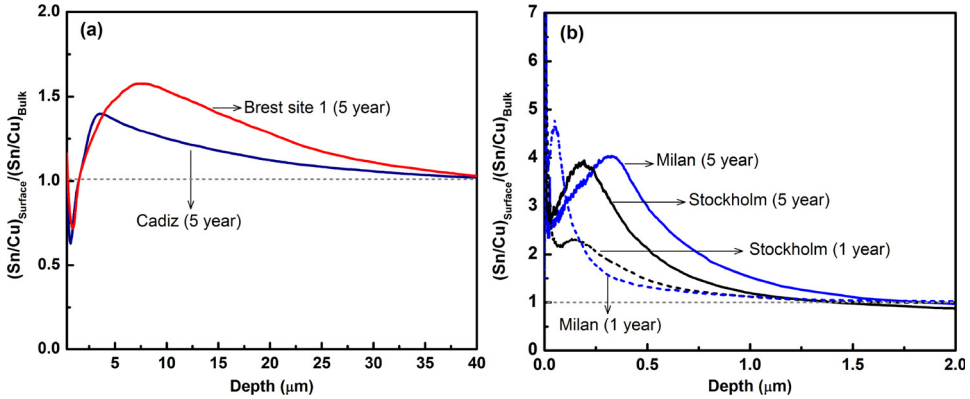

Fig. 12. Enrichment of Sn compared with Cu in the patina compared with the corresponding bulk mass ratio determined by means of GDOES for Cu4Sn (Brest, Milan, Stockholm–1 and 5 years) and Cu6Sn (Cadiz–5 years).

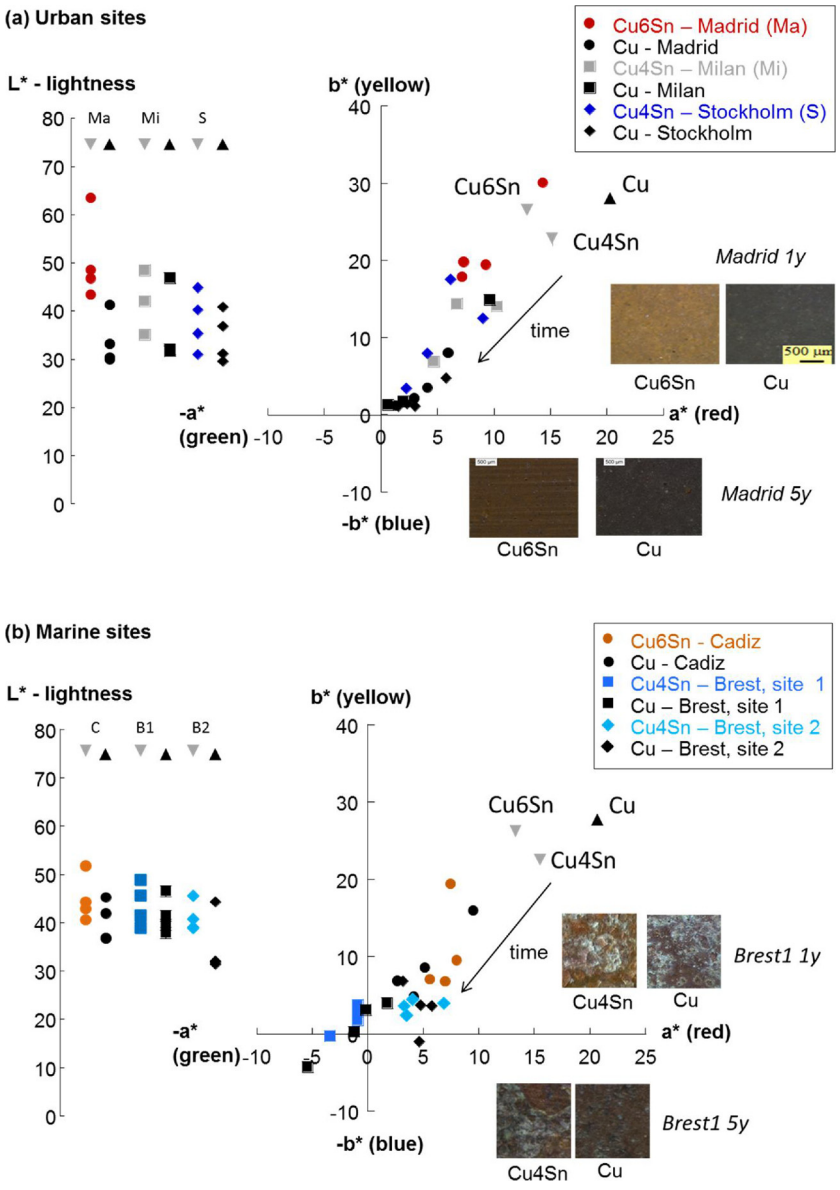

Fig. 13. Changes in surface appearance by means of colorimetry and selected stereo micrographs of Cu4Sn/Cu6Sn compared with Cu metal exposed up to 5 years at three urban (Madrid-Ma, Spain; Milan-Mi, Italy; Stockholm-S, Sweden) (a) and two marine sites (Cadiz-C, Spain; Brest sites 1-B1 and 2-B2, France). The black and grey triangles illustrate non-exposed surfaces. Based on the CIELab color reference space, surface appearance is described by the three coordinates, a* (red/magenta-green), b* (yellow-blue) and L* (lightness – black to white) (For interpretation of the references to colour in this figure legend, the reader is referred to the web version of this article.).

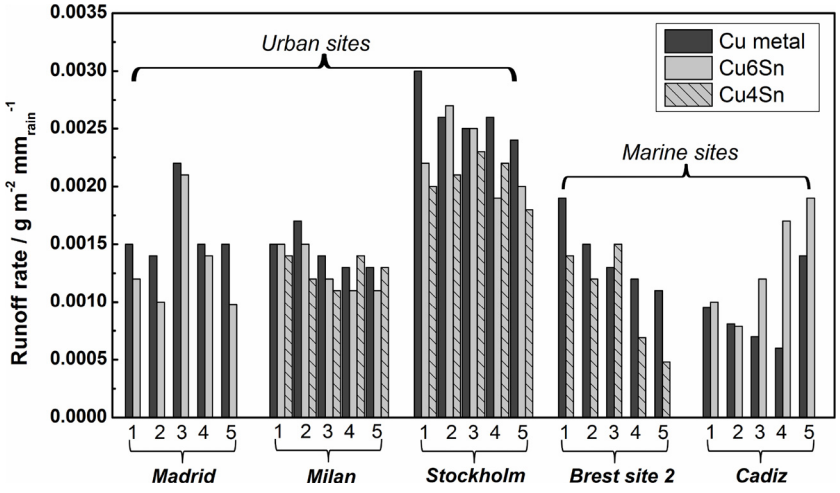

Fig. 14. Annual runoff rates of Cu normalized on geometric surface area and annual rainfall quantity for Cu metal and Sn-bronzes (Cu4Sn, Cu6Sn) exposed at unsheltered conditions at 45° from the horizontal, facing south at urban (a) and marine sites (b) up to 5 years.
Average annual rainfall quantities during the exposure period (Milan-620 mmy^{-1}; Madrid-315 mmy^{-1}; Stockholm 570 mmy^{-1}; Cadiz- 450 mmy^{-1}; Brest-800 mmy^{-1}).

presence of Sn oxides in streaks within the patina are of minor importance for the runoff process. More important are the corrosion product composition and surface coverage of Sn- *vs.* Cu-rich corrosion products at the outmost surface predominantly Cu-rich at both the urban (less than 6% Sn-oxides according to XPS findings) and the marine (no Sn-oxides) sites after 5 years of exposure. An increased surface coverage of Sn-rich corrosion products is believed to reduce the runoff rate of Cu, *e.g.* during a rain event succeeding flaking of the outermost Cu-rich corrosion products at the marine site. Similar runoff rates of Cu observed for Cu4Sn and Cu6Sn compared with Cu metal imply that the predictive runoff rate model, elaborated to assess the extent of released Cu from outdoor constructions at urban sites (the model is not valid for sites of high deposition rates of chlorides) also is applicable for Sn bronzes [37,58,59]. Information on total amounts of released Cu is though not sufficient for environmental risk assessments as such deliberations require knowledge of the chemical speciation of released Cu and its changes and fate upon environmental entry [37,60].

Slightly higher release rates of Cu were observed for the least-polluted site of Stockholm ($SO_2 < 3\,\mu g\,m^{-3}$) compared with the other sites. Similar findings have been observed for parallel studies on brass (15, 20 wt.% Zn) exposed at the same sites [44]. As discussed above for the corrosion rates, this is mainly attributed to the large differences in daily wet/dry conditions (*i.e.* dissolution/re-precipitation processes) and a high frequency of low-intensity rain events that result in longer contact periods between impinging rain water and the patina, conditions that increase the contribution of the first flush effect during single rain events and hence the total annual runoff quantity [61].

In all, in contrast with findings for the corrosion rates, Section 3.3, alloying with Sn does not influence the annual Cu runoff rate neither at urban nor the marine sites of this study. The reason is that the runoff process is governed by chemical reactions taking place at the outermost surface being predominantly composed of Cu-rich corrosion products, the same as formed on Cu metal, with only minor amounts of Sn-oxides at the outermost surface region, see Section 3.4. The presence of Sn-oxides within the patina and the patina morphology is of minor importance for the runoff process.

4. Summary

Thorough multi-analytical investigations employing different microscopic, spectroscopic, electrochemical and chemical tools have been performed to assess the role of Sn on the atmospheric corrosion performance of binary Cu-Sn bronze alloys (4, 6 wt.% Sn) compared with Cu metal used in contemporary outdoor architecture. Differences in microstructure and native surface oxide composition as well as patina evolution, corrosion rate, appearance and metal release at different urban and marine sites in Europe up to 5 years are highlighted. The results clearly show a beneficial effect of Sn compared with copper metal from a corrosion perspective at the urban sites with lower corrosion rates, the formation of thinner adherent patinas and different surface appearance as a result of the presence of Sn-oxides within and at the alloy/patina interface. No favorable effects of Sn alloying and the presence of Sn-oxides were observed at the marine sites showing similar or even thicker patinas with outer layers of poorly adherent corrosion products compared with Cu metal. Despite differences in corrosion rates and patina characteristics between the bronze alloys and Cu metal, and between different exposure conditions (urban and marine sites), no differences in copper release levels were observed due to similar corrosion products at the outmost surface.

Data availability

The raw/processed data required to reproduce these findings cannot be shared at this time due to legal or ethical reasons as it refers to an industrial project.

Acknowledgements

The European Copper Institute, Brussels, Belgium and the Scandinavian Copper Development Association are highly acknowledged for financial support, providing material and giving valuable comments. We are also grateful to Oskar Karlsson and Mats Randelius at Swerea Kimab, Stockholm Sweden for help with SEM/EDS imaging and GDOES analyses. S. Jafarzadeh, J. Brunk and J. Sandberg, former PhD-students at KTH, are highly acknowledged for help with the field exposures. The authors would like to express their sincere gratitude to the China Scholarship Council for supporting Tingru Chang's stay at KTH Royal Institute of Technology, Sweden.

Appendix A. Supplementary data

Supplementary material related to this article can be found, in the online version, at doi:https://doi.org/10.1016/j.corsci.2019.01.002.

References

[1] H.E. Boyer, T.L. Gall, Metals Handbook; Desk Edition, United States (1985).
[2] M.C. Squarcialupi, G.P. Bernardini, V. Faso, A. Atrei, G. Rovida, Characterisation by XPS of the corrosion patina formed on bronze surfaces, J. Cult. Heritage 3 (2002) 199–204.
[3] H. Ling, Q. Zhao, G. Min, Characterization of corroded bronze Ding from the Yin Ruins of China, Corros. Sci. 49 (2007) 2534–2546.
[4] G. Ingo, T. De Caro, C. Riccucci, E. Angelini, S. Grassini, S. Balbi, P. Bernardini, D. Salvi, L. Bousselmi, M. Gener, Large scale investigation of chemical composition, structure and corrosion mechanism of bronze archeological artefacts from Mediterranean basin, Appl. Phys. A 83 (2006) 513–520.
[5] T.E. Graedel, K. Nassau, J.P. Franey, Copper patinas formed in the atmosphere—I. Introduction, Corros. Sci. 27 (1987) 639–657.
[6] E. Paparazzo, L. Moretto, X-ray photoelectron spectroscopy and scanning Auger microscopy studies of bronzes from the collections of the Vatican Museums, Vacuum 55 (1999) 59–70.
[7] L. Robbiola, J.-M. Blengino, C. Fiaud, Morphology and mechanisms of formation of natural patinas on archaeological Cu–Sn alloys, Corros. Sci. 40 (1998) 2083–2111.
[8] R. Tylecote, The effect of soil conditions on the long-term corrosion of buried tin-bronzes and copper, J. Archaeol. Sci. 6 (1979) 345–368.
[9] F. Schweizer, Bronze Objects From Lake Sites: From Patina to Biography, Ancient and Historic Metals: Conservation and Scientific Research, Getty Conservation Institute, 1994, pp. 33–50.
[10] J. Wharton, R. Barik, G. Kear, R. Wood, K. Stokes, F. Walsh, The corrosion of nickel–aluminium bronze in seawater, Corros. Sci. 47 (2005) 3336–3367.
[11] A. Drach, I. Tsukrov, J. DeCew, J. Aufrecht, A. Grohbauer, U. Hofmann, Field studies of corrosion behaviour of copper alloys in natural seawater, Corros. Sci. 76 (2013) 453–464.
[12] J.H. Payer, Bronze Corrosion: Rates and Chemical Processes, the Conservation of Bronze Sculpture in the Outdoor Environment: a Dialogue Among Conservators, Curators, Environmental Scientists, and Corrosion Engineers, National Association of Corrosion Engineers, Houston, Texas, United States, 1992, pp. 103–121.
[13] C. Chiavari, K. Rahmouni, H. Takenouti, S. Joiret, P. Vermaut, L. Robbiola, Composition and electrochemical properties of natural patinas of outdoor bronze monuments, Electrochim. Acta 52 (2007) 7760–7769.
[14] D. Šatovića, L. Valek Žuljb, V. Desnica, S. Fazinić, S. Martinez, Corrosion evaluation and surface characterization of the corrosion product layer formed on Cu–6Sn bronze in aqueous Na_2SO_4 solution, Corros. Sci. 51 (2009) 1596–1603.
[15] N. Souissi, E. Sidot, L. Bousselmi, E. Triki, L. Robbiola, Corrosion behaviour of Cu–10Sn bronze in aerated NaCl aqueous media–electrochemical investigation, Corros. Sci. 49 (2007) 3333–3347.
[16] J. Muller, B. Laïk, I. Guillot, α-CuSn bronzes in sulphate medium: influence of the tin content on corrosion processes, Corros. Sci. 77 (2013) 46–51.
[17] I. Mabille, A. Bertrand, E. Sutter, C. Fiaud, Mechanism of dissolution of a Cu–13Sn alloy in low aggressive conditions, Corros. Sci. 45 (2003) 855–866.
[18] X. Zhang, I. Odnevall Wallinder, C. Leygraf, Mechanistic studies of corrosion product flaking on copper and copper-based alloys in marine environments, Corros. Sci. 85 (2014) 15–25.
[19] I. Odnevall Wallinder, X. Zhang, S. Goidanich, N. Le Bozec, G. Herting, C. Leygraf, Corrosion and runoff rates of Cu and three Cu-alloys in marine environments with increasing chloride deposition rate, Sci. Total Environ. 472 (2014) 681–694.
[20] D. Knotkova, K. Kreislova, Atmospheric corrosion and conservation of copper and bronze, WIT Transactions on State of the Art in Science and Engineering, (2007), pp. 107–142 Southampton.
[21] D. Knotkova, J. Vlckova, K. Kreislova, J. Had, Atmospheric corrosion of bronze and copper statues, roofs and cladding on Prague's monuments, Proc. of Art' 96, (1996).
[22] R. Picciochi, A.C. Ramos, M.H. Mendonça, I.T.E. Fonseca, Influence of the environment on the atmospheric corrosion of bronze, J. Appl. Electrochem. 34 (2004) 989–995.
[23] A.G. Nord, K. Trobber, A.J. Boyce, Atmospheric bronze and copper corrosion as an environmental indicator. A study based on chemical and sulphur isotope data,

Water Air Soil Pollut. 127 (2001) 193–204.
[24] T. Graedel, Copper patinas formed in the atmosphere—II. A qualitative assessment of mechanisms, Corros. Sci. 27 (1987) 721–740.
[25] A. Krätschmer, I. Odnevall Wallinder, C. Leygraf, The evolution of outdoor copper patina, Corros. Sci. 44 (2002) 425–450.
[26] M. Ghoniem, The characterization of a corroded egyptian bronze statue and a study of the degradation phenomena, Int. J. Conserv. Sci. 2 (2011).
[27] D.A. Scott, A review of copper chlorides and related salts in bronze corrosion and as painting pigments, Stud. Conserv. 45 (2000) 39–53.
[28] M. Serghini-Idrissi, M. Bernard, F. Harrif, S. Joiret, K. Rahmouni, A. Srhiri, H. Takenouti, V. Vivier, M. Ziani, Electrochemical and spectroscopic characterizations of patinas formed on an archaeological bronze coin, Electrochim. Acta 50 (2005) 4699–4709.
[29] F. Ospitali, C. Chiavari, C. Martini, E. Bernardi, F. Passarini, L. Robbiola, The characterization of Sn-based corrosion products in ancient bronzes: a Raman approach, J. Raman Spectrosc. 43 (2012) 1596–1603.
[30] W.A. Oddy, N.D. Meeks, Unusual phenomena in the corrosion of ancient bronzes, Stud. Conserv. 27 (1982) 119–124.
[31] T. Chang, I. Odnevall Wallinder, Y. Jin, C. Leygraf, The golden alloy Cu-5Zn-5Al-1Sn: a multi-analytical surface characterization, Corros. Sci. 131 (2018) 94–103.
[32] T. Chang, G. Herting, Y. Jin, C. Leygraf, I. Odnevall Wallinder, The golden alloy Cu-5Zn-5Al-1Sn: patina evolution in chloride-containing atmospheres, Corros. Sci. 133 (2018) 190–203.
[33] C. Leygraf, I. Odnevall Wallinder, J. Tidblad, T. Graedel, Atmospheric Corrosion, 2nd ed., John Wiley & Sons, 2016.
[34] S. Goidanich, I. Odnevall Wallinder, G. Herting, C. Leygraf, Corrosion induced metal release from copper based alloys compared to their pure elements, Corros. Eng. Sci. Technol. 43 (2008) 134–141.
[35] M.T. Sougrati, S. Jouen, B. Hannoyer, A. Barbier, A study of copper and copper alloys runoff in urban atmosphere, Proceedings of the International Conference Copper, (2006), pp. 12–15.
[36] G. Herting, S. Goidanich, I. Odnevall Wallinder, C. Leygraf, Corrosion-induced release of Cu and Zn into rainwater from brass, bronze and their pure metals. A 2-year field study, Environ. Monit. Assess. 144 (2008) 455–461.
[37] Y.S. Hedberg, J.F. Hedberg, G. Herting, S. Goidanich, I. Odnevall Wallinder, Critical review: copper runoff from outdoor copper surfaces at atmospheric conditions, Environ. Sci. Technol. 48 (2014) 1372–1381.
[38] S. Goidanich, J. Brunk, G. Herting, M. Arenas, I. Odnevall Wallinder, Atmospheric corrosion of brass in outdoor applications: patina evolution, metal release and aesthetic appearance at urban exposure conditions, Sci. Total Environ. 412 (2011) 46–57.
[39] ISO 9226: Corrosion of Metals and Alloys – Corrosivity of Atmospheres – Determination of Corrosion Rate of Standard Specimens for the Evaluation of Corrosivity, International Organization for Standardization, Geneva, Switzerland, 2012.
[40] ISO 17752: Corrosion of Metals and Alloys – Procedures to Determine and Estimate Runoff Rates of Metals From Materials as a Result of Atmospheric Corrosion, International Organization for Standardization, Geneva, Switzerland, 2012.
[41] W. He, I. Odnevall Wallinder, C. Leygraf, A comparison between corrosion rates and runoff rates from new and aged copper and zinc as roofing material, Water Air Soil Pollut. Focus 1 (2001) 67–82.
[42] K. Shimizu, G. Brown, H. Habazaki, K. Kobayashi, P. Skeldon, G. Thompson, G. Wood, Glow discharge optical emission spectrometry (GDOES) depth profiling analysis of anodic alumina films—a depth resolution study, Surf. Interface Anal. 27 (1999) 24–28.
[43] T. Aastrup, C. Leygraf, Simultaneous infrared reflection absorption spectroscopy and quartz crystal microbalance measurements for in situ studies of the metal/atmosphere interface, J. Electrochem. Soc. 144 (1997) 2986–2990.
[44] T. Chang, Y. Jin, L. Wen, C. Zhang, C. Leygraf, I. Odnevall Wallinder, J. Zhang, Synergistic effects of gelatin and convection on copper foil electrodeposition, Electrochim. Acta 211 (2016) 245–254.
[45] H. Gil, C. Leygraf, Quantitative in situ analysis of initial atmospheric corrosion of copper induced by acetic acid, J. Electrochem. Soc. 154 (2007) C272–C278.
[46] A. Doménech-Carbó, M.T. Doménech-Carbó, F.M. Valle-Algarra, J.V. Gimeno-Adelantado, L. Osete-Cortina, F. Bosch-Reig, On-line database of voltammetric data of immobilized particles for identifying pigments and minerals in archaeometry, conservation and restoration (ELCHER database), Anal. Chim. Acta 927 (2016) 1–12.
[47] C. Deslouis, O. Mattos, M. Musiani, B. Tribollet, Comments on mechanisms of copper electrodissolution in chloride media, Electrochim. Acta 38 (1993) 2781–2783.
[48] O. Barcia, O. Mattos, N. Pebere, B. Tribollet, Mass-transport study for the electrodissolution of copper in 1M hydrochloric acid solution by impedance, J. Electrochem. Soc. 140 (1993) 2825–2832.
[49] E. Sidot, N. Souissi, L. Bousselmi, E. Triki, L. Robbiola, Study of the corrosion behaviour of Cu–10Sn bronze in aerated Na_2SO_4 aqueous solution, Corros. Sci. 48 (2006) 2241–2257.
[50] A. Haseeb, H. Masjuki, L. Ann, M. Fazal, Corrosion characteristics of copper and leaded bronze in palm biodiesel, Fuel Process. Technol. 91 (2010) 329–334.
[51] S. Jouen, B. Hannoyer, O. Piana, Non-destructive surface analysis applied to atmospheric corrosion of tin, Surf. Interface Anal. 34 (2002) 192–196.
[52] T. Kosec, P. Ropret, A. Legat, Raman investigation of artificial patinas on recent bronze–part II: urban rain exposure, J. Raman Spectrosc. 43 (2012) 1587–1595.
[53] R.L. Frost, Raman spectroscopy of selected copper minerals of significance in corrosion, Spectrochim. Acta, Part A 59 (2003) 1195–1204.
[54] N. Dharmaraj, C. Kim, K. Kim, H. Kim, E.K. Suh, Spectral studies of SnO2 nanofibres prepared by electrospinning method, Spectrochim. Acta, Part A 64 (2006) 136–140.
[55] I. Odnevall Wallinder, C. Leygraf, A critical review on corrosion and runoff from zinc and zinc-based alloys in atmospheric environments, Corrosion 73 (2017) 1060–1077.
[56] J. Tidblad, C. Leygraf, V. Kucera, Acid deposition effects on materials: evaluation of electric contact materials after 4 years of exposure, Atmospheric Corrosion, ASTM International, 1995.
[57] S. Jouen, B. Hannoyer, A. Barbier, J. Kasperek, M. Jean, A comparison of runoff rates between Cu, Ni, Sn and Zn in the first steps of exposition in a French industrial atmosphere, Mater. Chem. Phys. 85 (2004) 73–80.
[58] I. Odnevall Wallinder, B. Bahar, C. Leygraf, J. Tidblad, Modelling and mapping of copper runoff for Europe, J. Environ. Monit. 9 (2007) 66–73.
[59] I. Odnevall Wallinder, S. Bertling, X. Zhang, C. Leygraf, Predictive models of copper runoff from external structures, J. Environ. Monit. 6 (2004) 704–712.
[60] I. Odnevall Wallinder, Y. Hedberg, P. Dromberg, Storm water runoff measurements of copper from a naturally patinated roof and from a parking space. Aspects on environmental fate and chemical speciation, Water Res. 43 (2009) 5031–5038.
[61] K. Athanasiadis, H. Horn, B. Helmreich, A field study on the first flush effect of copper roof runoff, Corros. Sci. 52 (2010) 21–29.